photonics

MDPI

Article

Research on the Ablation Characteristics and Thermomechanical Coupling Matching of Continuous-Wave/Pulsed Combined Lasers

Jing Xiao [1,2], Guoying Feng [1,*], Gang Ren [2], Jinhua Han [1], Huijun Xia [2], You Wang [2], Wantao Deng [2], Tianyu Chen [2] and Rongjun Guo [2]

[1] College of Electronics and Information Engineering, Sichuan University, Chengdu 610065, China
[2] Southwest Institute of Technical Physics, Chengdu 610041, China
* Correspondence: guoing_feng@scu.edu.cn

Abstract: In laser processing and electro-optical countermeasures, the laser ablation efficiency on the target is of great importance. Compared with traditional single laser irradiation, ablation by continuous-wave (CW)/pulsed combined laser has the advantages of high ablation efficiency, strong controllability, and low laser energy output requirements. However, current research on the synergistic mechanism and matching of combined laser irradiation requires improvement. In this study, damage experiments were mainly conducted on two modes of combined laser, CW/millisecond (CW/ms) and CW/nanosecond (CW/ns) laser. The temperature distribution, ablation rate, and ablation range under different irradiation conditions were tested quantitatively. The ablation characteristics and thermomechanical coupling matching of the combined laser were analysed and physically modelled. The results showed that compared with the pulsed laser alone, the ablation rate of the CW/ms combined mode was greater by approximately one order of magnitude, while that of the CW/ms combined mode was greater by approximately three orders of magnitude. Moreover, the thermomechanical coupling matching of the combined laser can be regarded as the matching of the impact pressure distribution of the pulsed laser with the range of the melting pool. The results of this study may offer guidance for further improving the synergistic enhancement damage mechanism of the combined laser.

Keywords: laser ablation; combined laser; thermomechanical coupling matching; damage mechanism

Citation: Xiao, J.; Feng, G.; Ren, G.; Han, J.; Xia, H.; Wang, Y.; Deng, W.; Chen, T.; Guo, R. Research on the Ablation Characteristics and Thermomechanical Coupling Matching of Continuous-Wave/Pulsed Combined Lasers. *Photonics* **2022**, *9*, 679. https://doi.org/10.3390/photonics9100679

Received: 28 July 2022
Accepted: 31 August 2022
Published: 21 September 2022

1. Introduction

The combined use of a continuous-wave (CW) and a pulsed laser (referred to as a combined laser) provides the target with both the continuous thermal effect damage of the CW laser and the mechanical effect damage of the pulsed laser [1–3], which can shorten the damage time and improve damage efficiency. With the advantages of high damage efficiency, strong controllability, and low laser energy output requirements, the combined laser is important for future laser applications, improving the ratio of efficiency to cost [4,5] and thus finding a wide range of potential applications in laser processing [6–9] and military fields [10]. Compared with single laser (using CW laser or pulsed laser alone), the interaction process of the combined laser with materials is more complicated. In addition to thermodynamic, ionisation, and plasma effects, this process involves thermomechanical coupling as well as parameter optimisation and matching, which adds further complexity to the physical mechanism. Current research mainly focuses on the experimental study of ablation characteristics, the physical modelling of ablation, and the optimisation and matching of laser parameters.

In terms of experiments and physical modelling, Cheng Yong et al. [11,12] tested and verified the enhanced damage effect of combined laser ablation, achieving an increase in material removal quality of an order of magnitude. Jia et al. [13] studied the influence of

the irradiation power of CW laser on the ablation effect. The experimental results revealed that with an increase in power, the ablation model transformed from the vaporisation recoil spatter of nanosecond (ns) pulsed laser to vaporisation recoil spatter and superheated boiling spatter. FOX [1] and Jiao Luguang et al. [14] studied the enhancement mechanism of CW laser irradiation, showing that CW lasers improved the laser absorptivity of the target, thus pulsed laser energy were more effectively deposited and utilised. In terms of laser parameter optimisation and matching, Jia et al. [15] experimentally studied the effect of the ns laser repetition rate on drilling efficiency in a CW/nanosecond (CW/ns) combined laser, achieving the highest drilling efficiency at a repetition rate of 10–25 kHz. Xiao Jing [16,17] analysed and compared spatial spot matching and time interval matching and found that the latter has a greater impact, mainly because the CW laser preheating time has a greater impact on the melting pool range and yield range. Lehane et al. [18] studied the influence of the time delay of pulsed laser relative to a CW laser on the ablation effect, which also revealed the importance of preheating time. Overall, the synergistic damage calculation model used for preheating to enhance the absorptivity has been preliminarily established, which provides a good reference for research on combined laser ablation. However, owing to the simplicity of the thermomechanical coupling model for enhancing melt removal, the internal relationship between the combined laser matching parameters and synergistic damage efficiency cannot be effectively established, resulting in the failure of quantitative design performance and optimisation of parameter matching. Meanwhile, the aforementioned research was conducted on a certain combined laser mode, and there lacks a comparative study for different combined modes. Therefore, it is extremely necessary to conduct a systematic study on the matching parameters and synergistic damage efficiency of different combined laser modes, analyse the influence of CW laser preheating time and the pulsed laser mechanical effect on the ablation effect of combined laser, and improve the synergistic enhancement damage mechanism model of the combined laser.

In this study, research was mainly conducted on the ablation effect of two modes of combined laser, CW/millisecond (CW/ms) and CW/ns, focusing on parameter matching in the two dimensions of time and energy. The internal relationship between the CW laser preheating time and synergistic damage, along with that between the pulsed laser mechanical effect and amplified synergistic damage effect damage, was obtained. Moreover, the influence of millisecond (ms) pulse width and ns pulse width on thermomechanical coupling matching was investigated, contributing to the improvement of the synergistic damage model of the combined laser.

2. Experimental System

To quantitatively test the ablation characteristics of the CW/pulsed combined laser, an experimental combined laser damage system was constructed, as shown in Figure 1.

The experimental system was mainly composed of a laser source system, timing control system, optical system, target, and testing equipment. The laser source system included a CW fiber laser (MFSC-1000W, Shenzhen Chuangxin Laser, Shenzhen, China), ms pulsed Nd:glass solid laser (HE-500, Southwest Institute of Technical Physics, Chengdu, China), and ns pulsed Nd:YAG solid laser (SGR-Extra-10, Beamtech Optronics, Beijing, China). The main output parameters of the laser source system are listed in Table 1. The timing control system was used to control the laser output mode and adjust the time matching of the combined laser. The laser output modes included continuous, pulsed, and combined laser. As shown in Figure 1b, in the combined laser output mode, the irradiation sequence and time interval of the CW and pulsed laser could be precisely controlled, and the pulsed laser was injected at the end of CW laser irradiation.

The optical system included a focusing lens and beam splitter, which were mainly used for spot size control in the two laser beams and monitoring of the laser power/energy. The CW and pulsed laser irradiated on the same position of the target at an angle of

approximately 8° through the focusing lens. The focusing laser spot diameter D was calculated based on Equation (1):

$$D = f \cdot \theta \quad (1)$$

where f is the focal length of lens; θ is the divergence angle of laser beam containing 86.5% of the total energy. A Focus Monitor (FM120, Primes, Hagen, Germany) was used to measure the divergence angle of the CW laser and a CCD camera (Laser Cam-HR, Coherent, CA, USA) was used to measure that of the ms and ns pulsed laser. For the CW/ms combined mode, the focal lengths of lenses were 4 m and 2 m, respectively, so the corresponding spot diameters were 8 mm and 5 mm, respectively. For the CW/ns combined mode, the focal lengths of lenses were 1.5 m and 1 m, respectively, so the corresponding spot diameters were 3 mm and 2 mm, respectively.

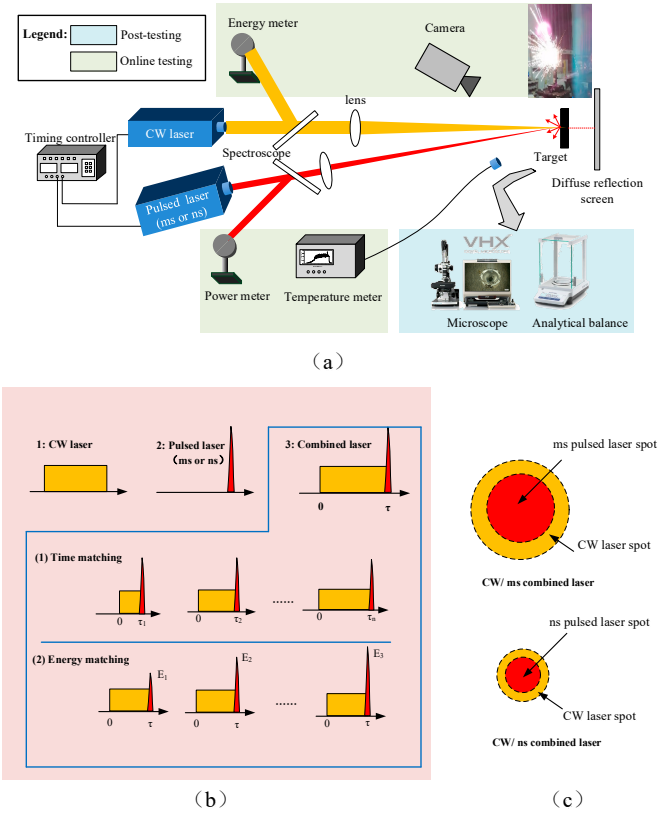

Figure 1. Experimental system. (**a**) Overall schematic diagram; (**b**) three modes of laser output and two modes of parameter matching; (**c**) combined laser spot.

Table 1. Main output parameters of laser source system.

Parameter	CW Laser	ms Pulsed Laser	ns Pulsed Laser
Wavelength	1.08 μm	1.06 μm	1.06 μm
Power	1000 W (max)	–	–
Energy @Pulse duration	–	500 J @1 ms	10 J @10 ns
Laser divergence angle	2 mard	2.5 mard	2 mard
	flat-top beam	flat-top beam	flat-top beam
Spot profile	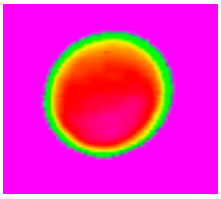	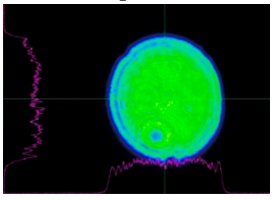	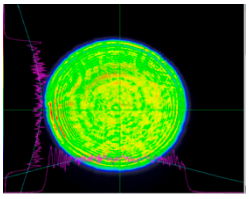

A 7075 aluminium alloy plate was adopted as the experimental target, with a diffuse reflector placed behind it to observe whether the target was perforated. The thermodynamic parameters of 7075 aluminium alloy are listed in Table 2. The test system included laser irradiation process detection and ablation result detection. The former included a power meter, energy meter, spot thermometer, and camera, and the latter included an analytical balance and microscope. During laser irradiation, a spot thermometer, KMGA740-L0, was used to measure the change in temperature, and a camera was used to record the laser damage process. The mass of the sample before and after laser ablation was measured using an analytical balance, METTLER TOLEDO ME, and the damage morphology was observed using an ultra-depth-of-field three-dimensional microscope system, Keyence VHX2000.

Table 2. Thermal parameters of 7075 aluminium alloy [19].

Temperature	Specific Heat Capacity	Density	Thermal Conductivity	Melting Point
373 K	900 J·(kg K)$^{-1}$	2775 kg·m^{-3}	142 W·(m K)$^{-1}$	748~908 K

3. Results

To study the enhancement mechanism of the combined laser in comparison with the single laser, single laser irradiation was first performed followed by combined laser irradiation. The ablation process and effect were compared and analysed.

3.1. CW Laser

Using a 2-mm thick target and CW laser irradiation for approximately 35 s in the 1-on-1 mode, we obtained the temperature evolution law and ablation morphology characteristics at different times during CW laser ablation, as shown in Figure 2.

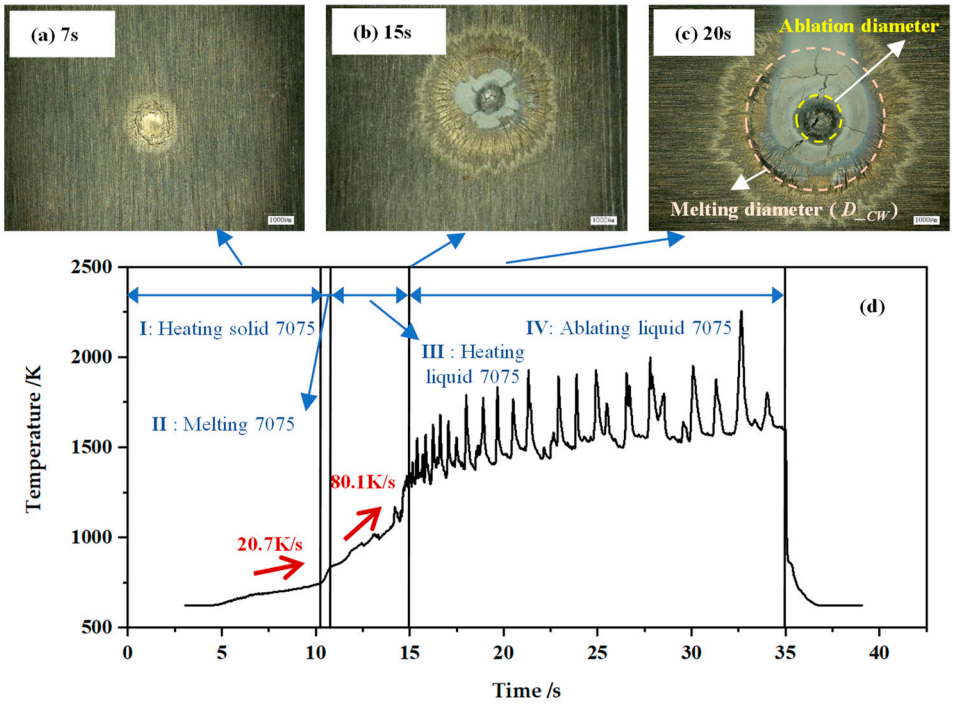

Figure 2. Evolution of temperature and ablation morphology during CW laser ablation. (**a**) Morphology at 7 s; (**b**) morphology at 15 s; (**c**) morphology at 20 s; (**d**) evolution of temperature.

As shown in Figure 2, according to the increasing temperature law of laser irradiation and the evolution characteristics of ablation morphology, the entire process from initial CW laser irradiation to target burn-through can be divided into four stages. Stage I (0~10.4 s), the solid-state heating stage: owing to the short laser irradiation time, the target had

not undergone a phase transition, the temperature increase rate of the test point was approximately 20.7 K/s; the aluminium alloy surface was softened via heating, and an annular plastic strain, such as "annular folds", was generated under the internal thermal stress, as shown in Figure 2a. Stage II (10.4~10.8 s), the phase transition stage: the target changed from solid to liquid, with the phase transition lasting for approximately 0.4 s. Stage III (10.4~15.0 s), the liquid heating stage: the metal target experienced a rapid increase in temperature, the laser absorptivity of the liquid aluminium alloy was higher than that of the solid aluminium alloy [20], leading to the rapid deposition of subsequent laser energy, and the temperature increase rate of the test point increased to 80.1 K/s. Stage IV (15~35 s), the oxidation reaction stage (in which oxygen participates due to ablation in the air): part of the liquid aluminium alloy experienced a violent oxidation reaction, white dust Al_2O_3 was produced during the combustion, and the ablation area was concentrated at the centre of the melted area, as shown in Figure 2c. At this stage, when the spot thermometer is working, more high-frequency noise may occur because the spattering oxides will interfere with the collection of incident laser and temperature measurement spectrum.

Laser ablation can be divided into longitudinal ablation in the direction of laser transmission and transverse ablation in the direction of the beam radius. The overall ablation and removal of the material can be analysed using Equation (2).

$$S = \frac{\triangle m}{E} = \frac{\triangle m}{P \cdot \tau} \tag{2}$$

where Δm is the mass removal or the mass difference of the target before and after laser irradiation, E is the laser energy, P is the laser power, and τ is the duration of CW laser irradiation.

Subsequently, the melting diameter $D_{\_cw}$ (as shown in Figure 2c), caused by the CW laser on the front surface of the target, and ablation rate were studied, as shown in Figure 3.

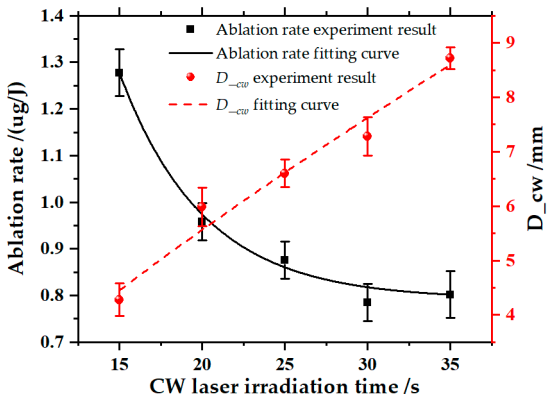

Figure 3. Ablation rate and melting diameter of an aluminium alloy plate irradiated by the CW laser over different irradiation times.

As shown in Figure 3, an increase in irradiation time resulted in an increase in the melting diameter and a decrease in the ablation rate. The mass ablation rate of the CW laser was low at approximately 0.8–1.3 μg/J. This shows that when CW laser is applied for ablation, the thermal conduction effect will cause diffusion and consumption of the absorbed energy, resulting in less energy being focused on the ablation and removal of the material.

3.2. Ms Pulsed Laser

The characteristics of the hole ablated using the ms pulsed laser indicate the strength of the mechanical effect. In this experiment, the 1-on-1 mode was adopted to study the relationship between the characteristics of the ablated hole in the target under ms pulsed laser irradiation and the pulse energy. The morphology of the ablated hole is shown in Figure 4.

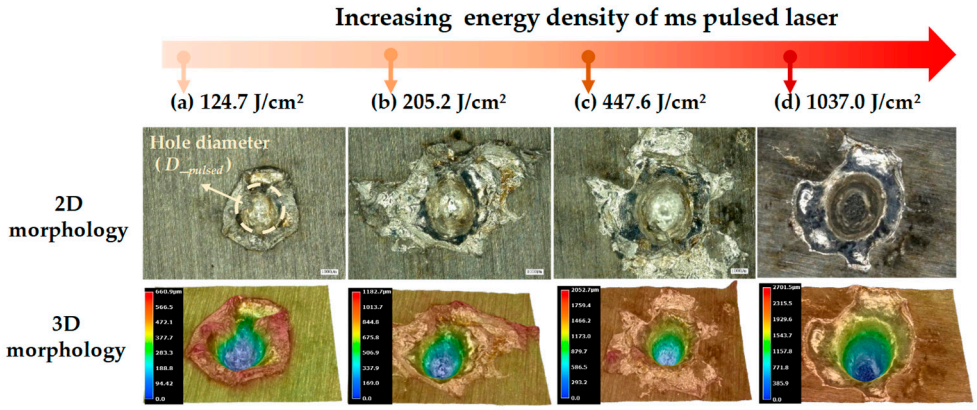

Figure 4. Morphology of the hole in the aluminium alloy plate ablated using the ms pulsed laser with different energy densities.

As shown in Figure 4, as the energy density of the ms pulsed laser increased, clear differences were found in the morphology of the ablated hole. When heated using the ms pulsed laser, the target melted and vaporised, and the high-temperature steam generated recoil vapour pressure, causing the melted substance to flow out of the melting pool. When the energy density was low, the recoil vapour pressure was small, and the melted substance was only pushed out of the melting pool and resolidified at its edge, as shown in Figure 4a. As the energy density increased, the range of the melting pool expanded, and the recoil vapour pressure also increased gradually. After the melted substance was pushed out of the melting pool, it resolidified around the pool as a spattering pattern, as shown in Figure 4b,c. When the energy density reached 1000 J/cm^2, the recoil vapour pressure enabled the melted substance to overcome the surface tension [21,22], which then separated, broke, and flew out of the melting pool opposite to the laser incident direction. The recast layer was barely visible at the edge of the melting pool, as shown in Figure 4d.

Under ms pulsed laser irradiation, the evolution of the ablated hole size and the ablation rate were closely related to the pulsed laser energy, which are shown in Figure 5.

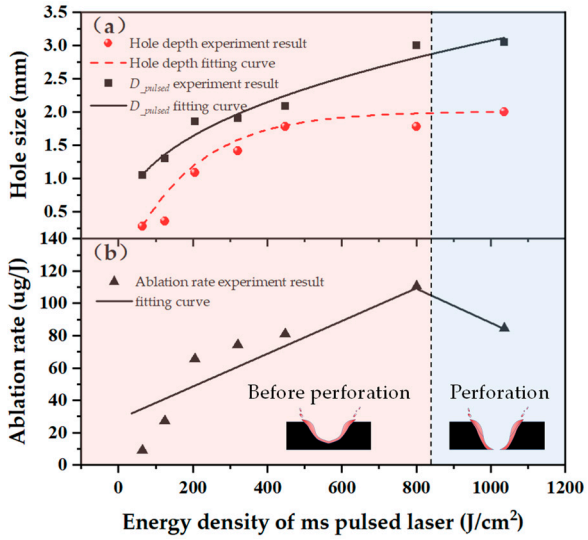

Figure 5. Variation in ablated hole size with ms pulsed laser energy. (**a**) Hole diameter and depth; (**b**) ablation rate.

As shown in Figure 5, before the target was perforated, the diameter, depth, and ablation rate of the ablated hole all increased with laser energy density. Their trends maintained a rapid then gradual increase before becoming flat. This indicates that ms pulsed laser ablation increased the depth and diameter of the ablated hole at the same time,

thus enhancing the utilisation of laser energy compared with that of the CW laser. When the energy density was approximately 1000 J/cm^2, the target was perforated, and part of the laser energy passed through the ablated hole, resulting in a reduction in the ablation rate. In general, under the irradiation of the ms pulsed laser (5 mm spot diameter), the diameter of the ablated hole ranges from 0 to 3 mm, and the ablation rate ranges from 8 to 110.7 μg/J. The ablation rate is well consistent with the earlier work of Gao et al., in which the experiment result is 6.7–121.8 μg/J [23].

3.3. CW/ms Combined Laser

The CW/ms combined laser damage experiment included two modes of parameter matching. First, time matching: the ms pulsed laser energy was kept constant (205.2 J/cm^2) to study the effect of CW laser irradiation time (τ: 5~25 s) on ablation efficiency. Second, energy matching: the CW laser irradiation time was kept constant (13 s) to study the effect of ms pulsed laser energy on ablation efficiency. Figure 6 shows the ablation rate results in the four cases: the CW laser, ms pulsed laser, combined laser time matching, and combined laser energy matching.

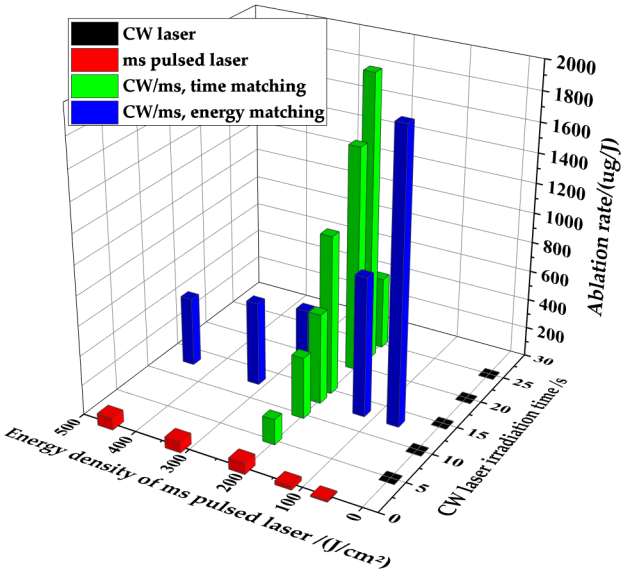

Figure 6. Ablation rate of the CW/ms combined laser.

As shown in Figure 6, when the 205.2 J/cm^2 ms pulsed laser was used alone, the ablation rate was 75.7 μg/J. However, under the irradiation of the CW/ms combined laser, the ablation rate of the ms pulsed laser was greatly enhanced to 170.4~1928.8 μg/J, with a maximum increase of 24.5 times.

Under combined laser irradiation, mass ablation rate can be greatly enhanced, and there are significant differences in ablation morphology. Tests were conducted on the damage morphologies generated by the CW laser (5~25 s, with an interval of 5 s), the ms pulsed laser (205.2 J/cm^2), and a combination of the two under different time matchings, as shown in Figure 7.

As shown by the damage morphology in Figure 7, the combined laser had greater damage efficiency than the single laser. Based on the damage morphology evolution characteristics of the combined laser under different time matchings, the ablation mechanism could be classified into three types, as shown in Figure 7c. Type I, insufficient thermal effect: when the CW laser preheating time was short (≤10 s), the target did not melt. Thus, when the pulsed laser irradiated, part of the energy was used to form a melting pool, whereas the other part was converted into the mechanical effect acting on the melting pool and causing mass removal. The thermomechanical coupling efficiency of the combined laser was low, and the target was not perforated. Type II, effectively matched thermomechanical

effect: when the CW laser preheating time was moderate (13~15 s), the mechanical effect of the ms pulsed laser could completely flush the melted substance out of the melting pool and remove it from the target surface, resulting in a smooth through-hole morphology and perforated target. Type III, insufficient mechanical effect: when the CW laser preheating time was long (≥20 s), the melting pool caused by the CW laser was too large. The mechanical effect of the ms pulsed laser could only flush part of the melted substance out of the melting pool, resulting in an irregular through-hole morphology and perforated target.

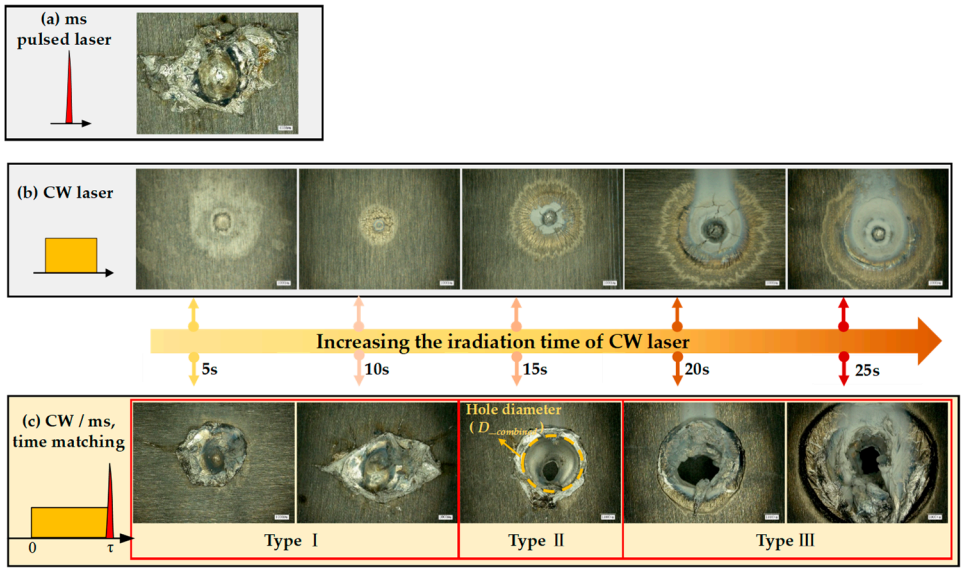

Figure 7. Ablation morphology. (**a**) Ms pulsed laser; (**b**) CW laser; (**c**) CW/ms combined laser.

To further clarify the causes of the three typical ablation mechanisms of the combined laser, research was conducted on the CW laser melting pool diameter ($D_{\_cw}$), the pulsed laser ablated hole diameter ($D_{\_pulsed}$), and the combined laser ablated hole diameter ($D_{\_combined}$), as shown in Figure 8. In general, the diameter of the pulsed laser ablated hole is approximately 2 mm. The CW laser melting pool diameter (with a maximum value of 7 mm) increased gradually with irradiation time. Under combined laser irradiation, the diameter of the ablated hole on the front surface of the target first increased and then decreased, ranging from 2 to 4 mm.

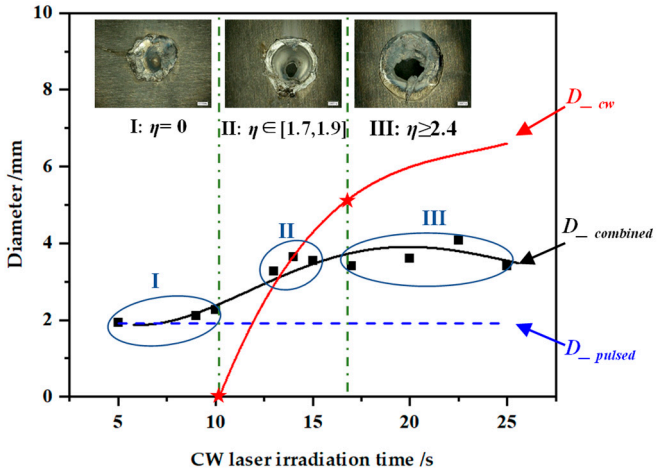

Figure 8. Melting diameter and hole size of the aluminium alloy under different laser parameters.

As shown in Figure 8, when the CW laser preheating time was less than 10 s, the thermal effect of the CW laser was insufficient, and $\eta = D_{\_cw} / D_{\_pulsed} = 0$. At this time, the damage morphology of the combined laser was similar to that of the pulsed laser,

resulting in Type I ablation. The size of the ablated hole caused by the combined laser was slightly larger than that of the ablated hole caused by the ms pulsed laser because CW laser preheating increases subsequent laser absorptivity. Between the preheating times of 13 s and 15 s, the diameter of the melting pool caused by the CW laser was larger than that of the ablated hole caused by the pulsed laser, and $\eta \in [1.7,1.9]$. The impact of the pulsed laser acted entirely on the melting pool, and the melted substance could be completely ejected from the pool under the impact pressure of vaporisation, realising efficient coupling in the thermomechanical effect of the combined laser. At these times, the diameter of the ablated hole caused by the combined laser was equivalent to the range of the melting pool caused by the CW laser, forming the Type II damage morphology. When the preheating time further increased, the range of the melting pool caused by the CW laser became too large and $\eta \geq 2.4$. The impact pressure could not completely remove the melt, resulting in a Type III damage morphology. As the melting pool expanded, the size of the through-hole first increased and then decreased. It can be concluded that the time matching of the combined laser can be regarded as the matching of the impact pressure of the pulsed laser with the range of the melting pool. Under the parameters used in this study, when the diameter of the melting pool caused by the CW laser did not exceed 1.9 times the diameter of the ablated hole caused by the pulsed laser, the mechanical effect of the pulsed laser could completely remove the melt.

By monitoring the temperature at the centre of the melting pool, it can be verified whether melting is completely removed. Figure 9a shows the variation in temperature with time at the centre point of the front surface under combined laser irradiation. The target was firstly heated under CW laser irradiation. At 13 s, the target temperature increased sharply owing to the application of the ms pulsed laser (Point A) and rapidly decreased to 828.8 K after pulsed laser irradiation ceased (Point B). Because the melting point of the 7075 aluminium alloy ranges from 748 to 908 K, the temperature measured by the spot thermometer at this time was that of the solid–liquid interface. Therefore, it was speculated that the impact pressure of the ms pulsed laser would remove almost all the melted substance from the melting pool. As shown in Figure 9b, which is a plot of the centre-point temperature at the end of pulsed laser irradiation (Point B) under different time matchings, when the preheating time did not exceed 15 s, the temperature of the melting pool under ms pulsed laser irradiation was always maintained within the melting point range of the material, indicating that the mechanical effect of the pulsed laser could completely remove the melt from the melting pool; when the preheating time was greater than 15 s, the test result of the spot thermometer was greater than the melting point range, indicating that the melted substance had not been completely removed. This is consistent with the results of previous analyses.

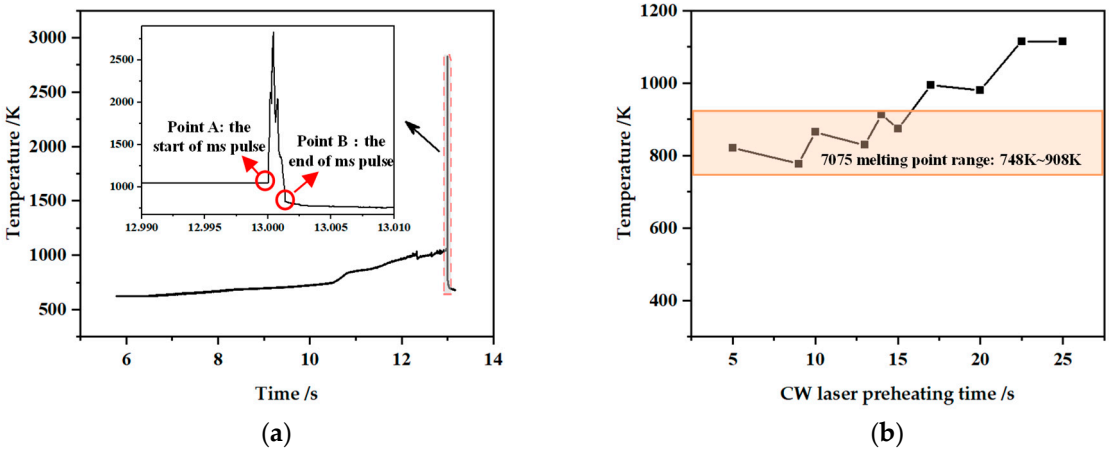

Figure 9. Temperature at the centre point of the front surface. (**a**) CW/ms combined laser irradiation mode when the CW laser preheating time (τ) equals 13 s; (**b**) temperature at the centre point at the end of pulsed laser irradiation under different preheating times.

3.4. CW/ns Combined Laser

An aluminium alloy with a thickness of 1 mm was adopted as the experimental target. Figure 10 shows the ablation rate of the target under four irradiation conditions: that is, the CW laser, ns pulsed laser, combined laser time matching, and combined laser energy matching. As shown in Figure 10, the ablation rate of the aluminium alloy irradiated by the CW laser ranged from 1.54 to 1.79 μg/J, and the ablation rate of the aluminium alloy irradiated by the ns pulsed laser ranged from 6.54 to 26.26 μg/J. After CW laser preheating, the ablation rate of the ns pulsed laser was enhanced to 1228.92~22319.47 μg/J, with a maximum increase of 849.9 times that of the ns pulsed laser alone.

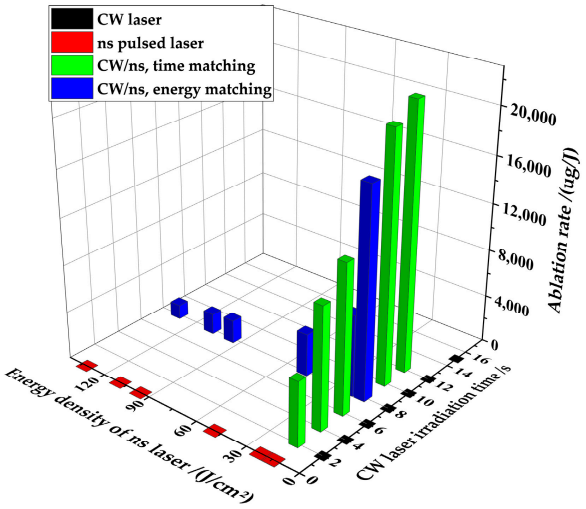

Figure 10. Ablation rate of the CW/ns combined laser.

The CW/ns combined laser greatly improved the ablation rate of the ns laser pulse and presented new features in the ablation morphology, as shown in Figure 11.

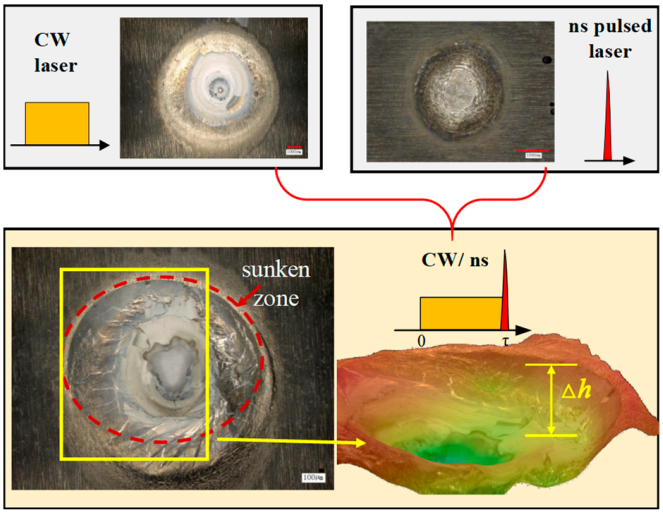

Figure 11. Damage morphologies of the aluminium alloy under three modes of laser output (CW laser, ns pulsed laser, and CW/ns combined laser).

Figure 11 shows the damage morphologies of the target in three cases, namely, with the CW laser (irradiation time of 8 s), ns pulsed laser (48.7 J/cm^2), and a combination of the two. When the CW laser irradiated the target for 8 s, a melting pool with a range of approximately 10 mm was generated on the target. A ns pulse was then added. Under its mechanical effect, the centre of the melting pool was perforated, with a perforation size of approximately 2 mm, equivalent to the spot size of the ns pulsed laser. At the same

time, the entire melting pool sunk towards the rear surface, resulting in a height difference (Δh) from the front surface of the target. This occurred because of the laser-supported detonation wave (LSDW) under ns pulsed laser irradiation, and the mechanical effect of LSDW diffusion caused the entire melting pool to sink towards the rear surface [24].

4. Discussion

Overall, the combined laser exhibited better ablation efficiency than the single laser. Moreover, there were differences in ablation enhancement and the thermomechanical coupling mechanism between the CW/ms and CW/ns combined laser. Figure 12 shows the ablation rates of the single laser and two modes of the combined laser. Compared with that of the pulsed laser alone, the ablation rate of the ns pulsed laser was approximately three orders of magnitude greater at 1228.92~22319.47 μg/J, whereas the ablation rate of the ms pulsed laser was approximately one order of magnitude greater at 170.4~1928.8 μg/J.

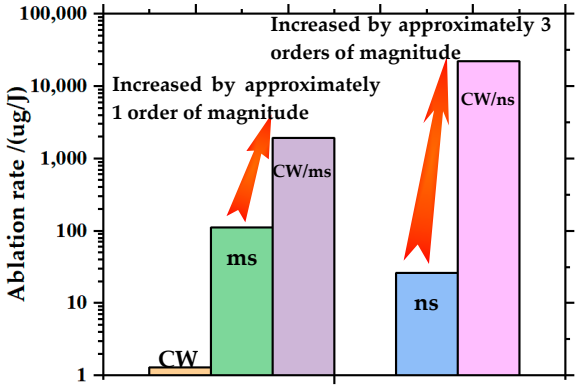

Figure 12. Comparison of the ablation rates of the two modes of the combined laser.

The significant difference in the ablation rates of the two modes of the combined laser was related to their thermomechanical coupling mechanisms. Under irradiation by the CW/ms combined laser, the rapid vaporisation of the target by the ms pulsed laser generated a recoil vapour pressure P_r, as shown in formula (3) [25]. The recoil vapour pressure acted on the melting pool, causing the melt to spatter. The mechanism model is shown in Figure 13a. In this experiment, the maximum temperature at the centre point of the target under CW/ms combined laser irradiation was approximately 3700 K. Using formula (3), the recoil vapour pressure generated by the ms pulse was calculated as 1.2 MPa. Under CW/ns combined laser irradiation, the target rapidly vaporised and ionised, resulting in a recoil vapour pressure (P_r,) and a pressure caused by the expansion of the LSDW (P_{LSDW}), as shown in Figure 13b. The temperature of the plasma plume reached more than 6500 K, according to which the recoil vapour pressure could be calculated to be no less than 67.6 MPa. Based on research by Qin et al. [26] in 2019, the shock wave pressure of ns pulsed laser is as high as GPa. Compared with the ms pulsed laser, the ns pulsed laser has a greater mechanical effect and higher efficiency in melt removal. Therefore, the combined use of the ns pulsed laser will achieve a better ablation effect on materials.

$$P_r = 0.55P_0 \exp[\frac{Lv}{R \cdot Tv}(1 - \frac{Tv}{T})] \quad (3)$$

where P_0 is the standard atmospheric pressure, L_v is the latent heat of vaporisation, R is the standard gas constant, T_v is the boiling point, and T is the temperature of vapour.

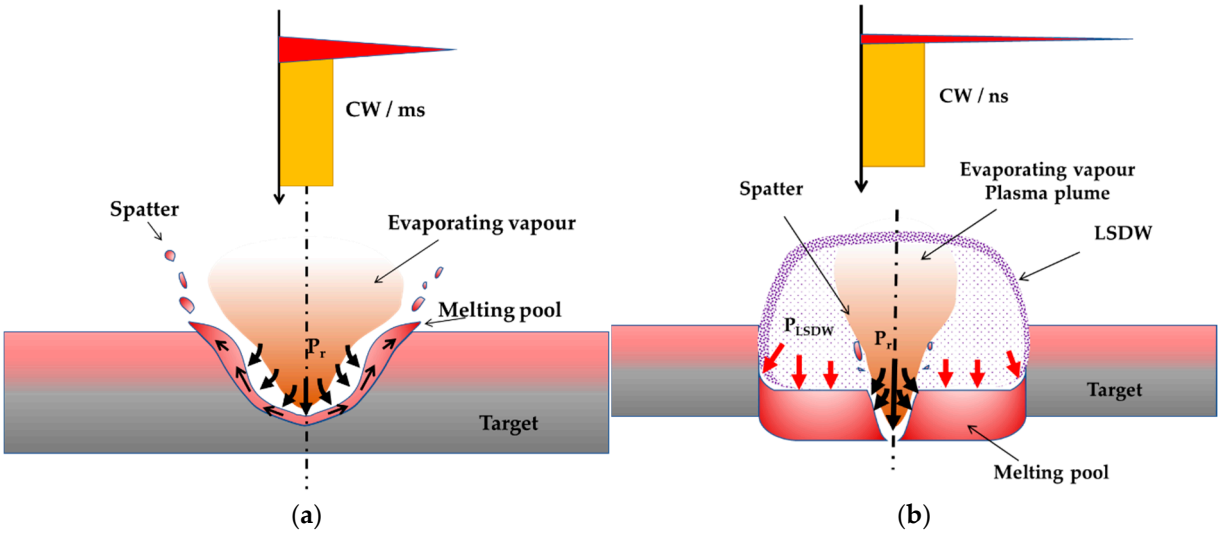

Figure 13. Thermomechanical coupling mechanism model of the two modes of the combined laser. (**a**) CW/ms; (**b**) CW/ns.

5. Conclusions

In this study, for two modes of the combined laser (CW/ms and CW/ns), quantitative tests were conducted on the temperature distribution, ablation rate, ablation size, and morphology under different conditions of irradiation, and research was performed on the ablation characteristics and thermomechanical coupling of the combined laser. The results were as follows: (1) CW laser preheating significantly improved the ablation rate of the pulsed laser. In the two modes of the combined laser, compared with the pulsed laser alone, the ablation rate of the ns pulsed laser was approximately three orders of magnitude greater at 1228.92~22319.47 μg/J, and the ablation rate of the ms pulsed laser was approximately one order of magnitude greater at 170.4~1928.8 μg/J. (2) The thermomechanical coupling matching of the combined laser can be regarded as the matching of the impact pressure distribution of the pulsed laser with the range of the melting pool. Under the laser parameters used in this study, when η was less than or equal to 1.9, the mechanical effect of the ms pulsed laser completely removed the melted material. When η exceeded 1.9, the mechanical effect was not sufficient to remove melted material. In follow-up research on the thermomechanical coupling mechanism model for enhancing the melt removal and parameter matching of the combined laser, emphasis should be placed on the spatial and temporal distribution of the mechanical impact of the pulsed laser and the dynamic melt process under this mechanical impact.

Author Contributions: Conceptualisation, J.X. and G.R.; methodology, G.F. and H.X.; validation, J.X., T.C. and R.G.; formal analysis, J.X.; investigation, J.H.; resources, Y.W.; data curation, W.D.; writing—original draft preparation, J.X.; writing—review and editing, J.X. All authors have read and agreed to the published version of the manuscript.

Funding: This research was funded by Key Laboratory of Plasma Physics Fund, grant no. 6142A04200210.

Informed Consent Statement: Not applicable.

Data Availability Statement: The data presented in this study are available on request from the corresponding author.

Conflicts of Interest: The authors declare no conflict of interest.

References

1. Fox, J.A. A method for improving continuous wave laser penetration of metal targets. *Appl. Phys. Lett.* **2008**, *26*, 682–684. [CrossRef]
2. Robin, J.E.; Nordin, P. Improved cw laser penetration of solids using a superimposed pulsed laser. *Appl. Phys. Lett.* **2008**, *29*, 3–5. [CrossRef]

3. Towle, L.C.; McKay, J.A.; Schriempf, J.T. The penetration of thin metal plates by combined cw and pulsedlaser radiation. *J. Appl. Phys.* **1979**, *50*, 4391–4393. [CrossRef]
4. Ding, Y.; Yang, L.; Hong, M. Enhancement of pulsed laser ablation assisted with continuous wave laser irradiation. *Sci. China Phys. Mech. Astron.* **2019**, *62*, 34211. [CrossRef]
5. Khalil, A.A.I.; Hafez, A.I.; Elgohary, M.E.; Morsy, M.A. Tungsten ion source under double-pulse laser ablation system. *Chin. Phys. B* **2017**, *26*, 095201. [CrossRef]
6. Kasuga, M.; Sano, T.; Hirose, A. Grain refining in weld metal using short-pulsed laser ablation during CW laser welding of 2024-T3 aluminum alloy. *Int. J. Extrem. Manuf.* **2019**, *1*, 045003. [CrossRef]
7. Hess, A.; Weber, R.; Heider, A.; Graf, T.J.P.P. Forced deep-penetration welding with low-power second-harmonic assistance of cw copper welding with 1 µm wavelength. *Phys. Procedia* **2010**, *5*, 29–36. [CrossRef]
8. Hess, A.; Schuster, R.; Heider, A.; Weber, R.; Graf, T.J.P.P. Continuous wave laser welding of copper with combined beams at wavelengths of 1030 nm and of 515 nm. *Phys. Procedia* **2011**, *12*, 88–94. [CrossRef]
9. Jia, X.; Chen, Y.; Liu, L.; Wang, C. Combined pulse laser: Reliable tool for high-quality, high-efficiency material processing. *Opt. Laser Technol.* **2022**, *153*, 108209. [CrossRef]
10. Zeng, J.; Lu, Q.; Shu, B.; Xu, X.; Liu, Z. Combined damage effect of GaAs irradiated by 1.06 µm CW and pulse laser. *High Power Laser Part. Beams* **1998**, *10*, 217–220.
11. Yong, C.; Mengzhen, Z.; Yunfeng, M.; Jingsong, W.; Xu, L.; Fangzheng, D.; Chaoyong, T.; Xia, C.; Yanlong, G.; Hua, C. Mechanism and effects of complex laser ablation. *Infrared Laser Eng.* **2016**, *45*, 1105005. [CrossRef]
12. Yong, C.; Yanlong, G.; Huang, T. Development trend of tactical laser weapons. *Laser Optoelectron. Prog.* **2016**, *53*, 110004.
13. Jia, X.; Zhang, Y.; Chen, Y.; Wang, H.; Zhu, G.; Zhu, X. Combined pulsed laser drilling of metal by continuous wave laser and nanosecond pulse train. *Int. J. Adv. Manuf. Technol.* **2019**, *104*, 1269–1274. [CrossRef]
14. Luguang, J.; Guomin, Z.; Minsun, C. Investigation on the irradiation effects of Q235 steel targets by combined laser. *Infrared Laser Eng.* **2011**, *40*, 848–852.
15. Jia, X.; Chen, Y.; Zhu, G.; Wang, H.; Aleksei, K.; Zhu, X. Experimental study on the optimum matching of CW-nanosecond combined pulse laser drilling. *Appl. Opt.* **2019**, *58*, 9105–9111. [CrossRef]
16. Xiao, J.; He, H.; Xia, H.; Jia, J. Temperature flied simulation on aluminium alloy irradiated by long pulsed laser and continuous wave laser. *Chin. J. Lasers* **2012**, *39*, 1103002. [CrossRef]
17. Xiao, J.; He, H.; Xia, H. Stress simulation of aluminium alloy irradiated by long pulsed laser and continuous wave laser. *Chin. J. Lasers* **2013**, *40*, 0803009. [CrossRef]
18. Lehane, C.; Kwok, H.S. Enhanced drilling using a dual-pulse Nd: YAG laser. *Appl. Phys. A* **2001**, *73*, 45–48. [CrossRef]
19. Editorial Board of the Practical Handbook of Engineering Materials. *Practical Handbook of Engineering Materials (Volume 3): Aluminium Magnesium Alloys*; China Standard Press: Beijing, China, 2002.
20. Zhang, K. Phase transition speed research of metal material at laser irradiation medium strength. *Acta Phys. Sin.* **2004**, *53*, 1815–1819. [CrossRef]
21. Yan, Z.; Mei, X.; Wang, W.; Pan, A.; Lin, Q.; Huang, C. Numerical simulation on nanosecond laser ablation of titanium considering plasma shield and evaporation-affected surface thermocapillary convection. *Opt. Commun.* **2019**, *453*, 124384. [CrossRef]
22. Zhang, G.; Zhu, B.; Zou, J.; Wu, Q.; Xiao, R. Correlation between the spatters and evaporation vapor on the front keyhole wall during fiber laser keyhole welding. *J. Mater. Res. Technol.* **2020**, *9*, 15143–15152. [CrossRef]
23. Heyan, G.; Xing, J.; Lan, L.; Meng, Y.; Ying, W. Effect of energy density on material migration mechanism in millisecond laser ablation of aluminum target. *Infrared Laser Eng.* **2021**, *50*, 20210264.
24. Zhang, Y.; Lu, X.; Zhou, M.-L.; Lin, X.-X.; Zheng, Z.-Y.; Li, Y.-T.; Zhang, J. Laser propulsion with a high specific impulse using a thin film propellant. *Chin. Phys. B* **2011**, *20*, 087901. [CrossRef]
25. Wang, L.; Zhang, Y.; Yan, W. Evaporation model for keyhole dynamics during additive manufacturing of metal. *Phys. Rev. Appl.* **2020**, *14*, 064039. [CrossRef]
26. Qin, Y.; Förster, D.J.; Weber, R.; Graf, T.; Yang, S. Numerical study of the dynamics of the hole formation during drilling with combined ms and ns laser pulses. *Opt. Laser Technol.* **2019**, *112*, 8–19. [CrossRef]